Transient Model to Study Voltage Distribution in Electrical Machine Windings Considering the Rotor

R. S. Ferreira, A. C. Ferreira

***Abstract*--Stator machine windings are submitted to transient overvoltages when a surge achieves the line-end coils. The study of transient voltage distribution between turns and coils is an important step for the effectiveness of the machine's design. Several previous works investigate this voltage distribution by using simulation models or by means of measurement results. Nevertheless, it was not found in the literature any work that takes the rotor into account. Therefore, this paper aims at verifying the influence of the rotor in the transient voltage distribution inside the machine by numerical simulations. To obtain the results a complete model is used, in which transient magnetic fields and electric circuit elements are coupled. The calculation of the electric circuit parameters and the performing of the transient simulations are done by using Finite Elements Method. The transient model of each individual coil of the model is validated by measurement results. The simulations show that the rotor, indeed, has influence in transient voltage distribution, mainly for the coils other than the first.**

***Keywords*: Electrical Machines, Transient Voltage Distribution, Finite Element Method (FEM), Rotor Transient Model.**

I. Introduction

IN normal operation condition, that is, under rated frequency, the turn-to-turn and coil-to-coil voltages in a stator winding are evenly distributed, which means that the amplitude and waveform of the voltage across the coils and across the turns are similar. Although, if a surge is applied to the line-end coil, it propagates into the windings and the voltage distribution is not any more evenly distributed.

The transient voltage created by the incident surge in the line-end coil can deteriorate the insulation system because of partial discharge activity [1][2]. Therefore, the knowledge of the amplitude and waveform of the transient overvoltage is of great importance for the main and turn insulations design.

Considering large machines with form wound coils, the focus of this paper, in the existent models the transient voltage distribution is obtained by using an equivalent lumped circuit or by means of multiconductor transmission line theory [3][4], which considers the parts of the machine, slot and end-windings regions, in series. The concept of multiconductor transmission line have been used in a recent work [5] to optimize the insulation design considering the transient voltage distribution.

Moreover, in [6] measurements in a form wound motor winding were performed, and the results are compared with a simulation model. The model uses finite elements method to calculate the parameters of the lumped equivalent circuit. In [7] measurement results of overvoltages between coils and turns are presented. In [8] the coil shape and insulation thickness influence on the transient voltage distribution have been investigated. In other work [8] the influence of the laminated core has been investigated. The results have shown that the solid core has presented underestimated results when compared with a laminated model.

Regarding the rotor, in [10] its influence on the turn-to-turn overvoltages has been briefly analysed using a single-coil model. At that time, it was concluded that the rotor has little influence on the maximum values for the interturn overvoltages, however the turn-to-ground voltages have not been analysed. In the most recent works, which investigate the transient voltage distribution in machine stator windings, the rotor is always neglected, in measurements and in simulation models.

In this context, this paper aims at verifying the influence of the rotor presence on the turn-to-turn and turn-to-ground transient voltage distributions by means of numerical simulations. To perform the simulations, it is used a model in which transient magnetic fields and electric circuit elements (lumped parameters) are coupled [11][12], by using Finite Elements Method to obtain the electric circuit elements and to perform the transient simulations. With this approach it is possible to consider the rotor in the model. The model of each individual coil is also validated by measurement results.

The main contributions of the paper are summarized as follows: simulations performed in a three-phase model including one winding group and; transient results that take the rotor into account in a detailed model which also analyses the turn-to-ground voltages.

II. Proposed Model

The numerical results presented in this paper are obtained by means of Finite Element Method (FEM). Transient simulations to calculate the interturn voltages are done considering a 2D geometry built in Ansys Maxwell software, as can be seen in Fig. 1, coupled with electric circuit elements. The main data of the motor used during the studies can be also seen in TABLE I.

This work was partially supported by INERGE (Instituto Nacional de Energia Elétrica), CNPq (Conselho Nacional de Desenvolvimento Científico e Tecnológico), CAPES (Coordenação de Aperfeiçoamento de Pessoal de Nível Superior) Finance Code 001 and FAPEMIG (Fundação de Amparo à Pesquisa do Estado de Minas Gerais).

R. S. Ferreira and A. C. Ferreira are with the Department of Electrical Engineering, Universidade Federal do Rio de Janeiro, COPPE/UFRJ, Rio de Janeiro, Brazil (e-mail: rodrigo.sousa@ufrj.br and ferreira@ufrj.br).

Paper submitted to the International Conference on Power Systems Transients (IPST2021) in Belo Horizonte, Brazil, June 6-10, 2021.

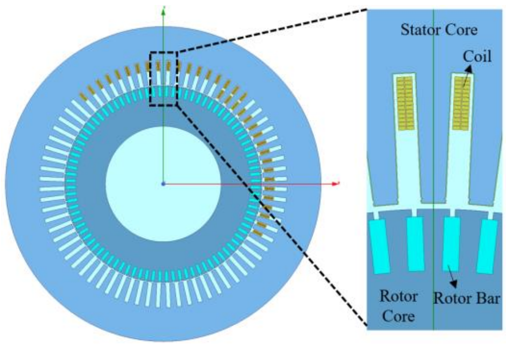

Fig. 1. 2D model used to perform the transient simulations.

TABLE I
MOTOR MAIN DATA.

Type	Squirrel Cage Induction
Rated Power [MW]	10
Rated Voltage [kV]	13.8
Winding	Double Layer
Connection	Isolated Star
Number of Turns per Coil	13
Number of Rotor Bars	88
Individual Conductors Size [mm x mm]	3.2 x 6.8
Main Insulation Thickness [mm]	3.0
Turn Insulation Thickness [mm]	0.3
Stator External Diameter [mm]	1580
Rotor External Diameter [mm]	989

In the transient simulation, magnetic fields are directly solved by FEM taking (1) into account for the 2D geometry presented in Fig. 1:

$$\delta \nabla \times \upsilon \nabla \times \boldsymbol{A} = J_s - \sigma \frac{\partial \boldsymbol{A}}{\partial t} - \sigma \nabla V + \sigma \boldsymbol{\vartheta} \times \nabla \times \boldsymbol{A} \qquad (1)$$

where υ is the magnetic reluctivity [m/H], $\boldsymbol{A}$ is magnetic vector potential [Wb/m], $\boldsymbol{J_s}$ is the current density source [A/m^2], σ is the electric conductivity [S/m], V is the voltage applied to the finite element region [V] and $\boldsymbol{\vartheta}$ is the relative velocity between the magnetic field and the conductors [m/s]. The right side of the previous equation represents the sources that can generate the magnetic field in the considered geometry. Moreover, each material of the geometry is modelled by the magnetic reluctivity and electrical conductivity.

According to Fig. 1, regarding the stator winding, each individual conductor is modelled, to take skin and proximity effects into account. The skin effect is computed directly by using (2):

$$\delta = \sqrt{2/(\omega \cdot \mu \cdot \sigma)} \qquad (2)$$

where δ is the penetration depth [m], ω is the angular frequency of the source of supply [rad/s] and μ is the magnetic permeability [H/m].

Considering that each individual conductor is modelled separately, the proximity effect is also directly considered by the solver, because during the simulation the magnetic flux generated by nearby conductors influences the total magnetic flux crossing each conductor.

Moreover, to simulate the transient overvoltage inside the motor it is necessary to consider the capacitance between turns and from turns-to-ground, which are not considered by the magnetic solver. Therefore, these capacitances are calculated and included in the magnetic transient solver as electric circuit elements. Furthermore, as it was used a 2D geometry, the end-windings are also considered as electric circuit elements.

Concerning the rotor, the same methodology is used, which means that the 2D geometry of the rotor bars are directly considered by the transient magnetic solver, as can be seen in Fig. 1. Moreover, the end ring and the rotor's capacitances are included as electric circuit elements.

Therefore, the model used to obtain the transient voltage distribution can be better explained by the equivalent circuits depicted by Fig. 2 and Fig. 3, which show the model used for each turn of the stator winding and for each bar of the rotor, respectively.

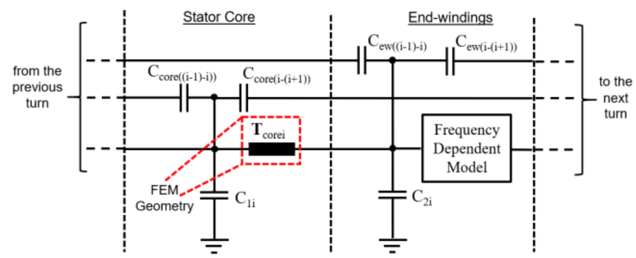

Fig. 2. Equivalent circuit for each stator turn.

As can be seen in Fig. 2, each stator turn is modelled as two "π" sections composed of elements in which the transient magnetic fields are directly solved by FEM, identified by T_{corei} (where "i" is the i-th turn), representing the portion of the turn located in the stator core, and electric circuit elements that are related to the stray capacitances and end-windings model. Moreover, according to Fig. 2 the series impedance of the end-windings for each turn is considered as a frequency-dependent model included in the simulations by electric circuit elements as explained later. Finally, the capacitances considered are the turn-to-turn ($C_{core(i-(i+1))}$ and $C_{core((i-1)-i)}$ for the stator core region and $C_{ew(i-(i+1))}$ and $C_{ew((i-1)-i)}$ for the end-windings region) and the turn-to-ground (C_{1i} and C_{2i}). According to the scheme the only turn-to-turn capacitances considered are related to adjacent turns of the same coil, because the other are much lower and they can be disregarded.

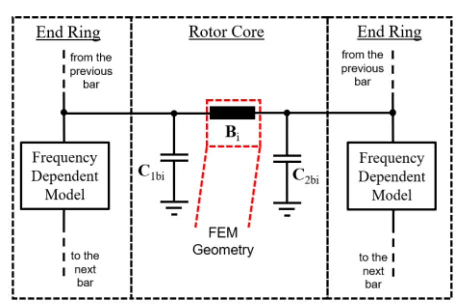

Fig. 3. Equivalent circuit for each rotor bar.

For the rotor model, according to Fig. 3, each bar (B_i, where "i" is the i-th bar of the rotor) is directly considered in the transient solver. The capacitances from the rotor-to-ground (C_{1bi} and C_{2bi}) are included as electric circuit elements. Moreover, for the end rings a frequency-dependent model is also considered.

In summary, for rotor and stator models, the electric circuit elements are calculated before the starting of the transient simulation and they are included between the conductors of the 2D geometry using the “Circuit Editor” from Ansys Maxwell. With this approach the transient magnetic simulation for the 2D geometry presented in Fig. 1 is coupled with electric circuit elements taking the stray capacitances and the regions not included in the 2D model (end-windings and end-rings) account. A general scheme for the complete model is shown in Fig. 4. The calculation of the electric circuit elements is explained in the next sub-sections. Moreover, the solvers indicated in the figure are specifically from Ansys Maxwell software.

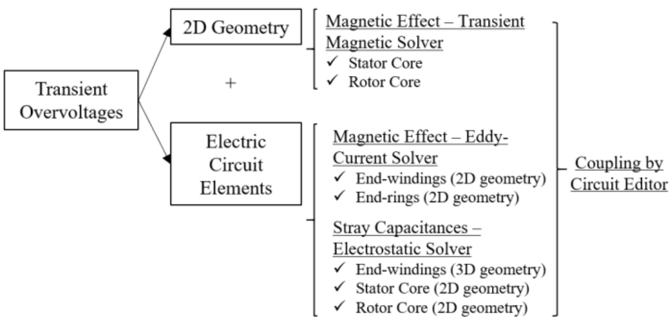

Fig. 4. Equivalent scheme for the complete model.

A. End-Windings

According to the previous section, the end-windings parameters need to be calculated to be included between the conductors of the transient model. In this paper they have been calculated as presented in [13].

Capacitances are calculated in the electrostatic frequency independent solver from Finite Element Method by using the 3D geometry of the coil shown in Fig. 5.

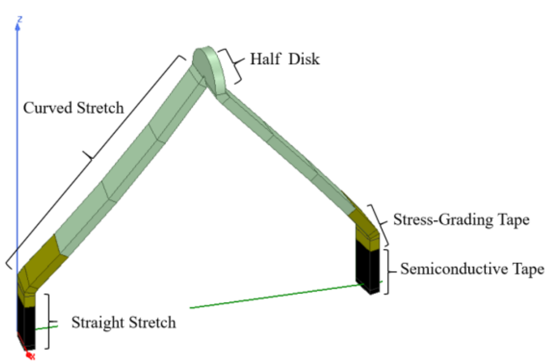

Fig. 5. 3D model used for the end-winding.

To calculate the turn-to-turn and the turn-to-ground capacitances the model shall consider each insulation part, that is, main and turn, geometrically separated. Moreover, the simulation considers the effect of the different insulations together. The capacitances are calculated by exciting each turn with a DC voltage and the external surface of the coil, where the semiconductive and stress-grading tapes are present, is grounded [13] as shown in Fig. 5. These excitations are also the boundary conditions for the electrostatic simulation. The main parameters used in the electrostatic solver is presented in TABLE II.

TABLE II

PARAMETERS USED TO CALCULATE THE CAPACITANCES.

Parameter	**Value**
Main Insulation Relative Permittivity	4.0
Turn Insulation Relative Permittivity	2.5

In TABLE IV the main results for the capacitances obtained are presented. According to the results the capacitances of non-adjacent turns can be neglected, as previously presented in Fig. 2.

Furthermore, according to Fig. 1, for the end-windings region, a frequency-dependent model with electric circuit elements (inductances and resistances) is considered for each turn, which can be seen in more details in Fig. 6.

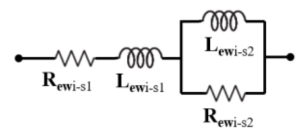

Fig. 6. Frequency-dependent model for the end-windings.

The model for each turn is based on works used to model electromagnetic transients in cables [14][15]. It consists of a fitting of the series impedance response as a function of frequency for each turn of the end-winding. First of all, a frequency response, for resistance and inductance, of each turn is required, and it is obtained as presented in a previous work [13], based on an eddy-current simulation of an equivalent 2D geometry. In this approach, the 3D model of the end-winding is considered as two parts: the part 1 is modelled as a straight coil and corresponds to the straight and curved stretches depicted in Fig. 5; the part 2 is modelled as an axisymmetric geometry and corresponds to the half disk depicted in Fig. 5. To obtain the resistance and inductance, each stranded conductor has been modelled to take skin and proximity effects into account [13].

For the simulations it is also necessary to know the magnetic permeability and electric conductivity of the materials. The insulation layers (main and turn insulations) are not considered in the simulations, since their electrical conductivities are very low compared to the copper conductors, whose values are indicated in TABLE III. To perform the simulations, the rated current is applied in each individual turns as excitation. Moreover, a balloon boundary condition has been considered, since there is no core in this region to confine the magnetic flux.

TABLE III

PARAMETERS USED TO CALCULATE INDUCTANCES AND RESISTANCES.

Material	Copper
Relative Permeability	1.0
Electric Conductivity [S/m]	$5.8 \cdot 10^{7}$

After calculating the series impedance frequency response of the turns, the parameters ($R_{ewi\text{-}s1}$, $R_{ewi\text{-}s2}$, $L_{ewi\text{-}s1}$, and $L_{ewi\text{-}s2}$) of the end-windings model, for each turn, are obtained as follows:

- $R_{ewi\text{-}s1}$: is the low-frequency resistance of the i-th turn, that is, the resistance for the lowest frequency considered;

- R_{ewi-s2}: is the difference between the high-frequency resistance (resistance calculated for the highest frequency) and low-frequency resistance of the i-th turn;
- L_{ewi-s1}: is the high-frequency inductance of the i-th turn;
- L_{ewi-s2}: is the difference between the low and the high-frequency inductances of the i-th turn.

It shall be highlighted that the extreme values of frequency used have to be chosen carefully, once the model parameters are calculated for these specific frequencies. In this paper, they were considered according to the frequency spectrum of the applied signal. Therefore, the low and high frequencies were chosen according to the FFT (Fast Fourier Transform) of the surge applied in the terminals of the machine, which in this paper is a simple ramp that can be considered as a trapezoidal pulse.

The frequency spectrum of a trapezoidal pulse depends on the rise time (t_{rise}). In general, the frequency response shows a maximum magnitude for 0 Hz (DC signal) and the maximum frequency is approximately equal to $1/t_{rise}$. Moreover, for frequencies higher than 100 kHz the amplitude is already lower than 6% of the DC amplitude for the rise time considered in this paper. Therefore, the lowest and highest frequencies used in this study are 0 Hz and 100 kHz, respectively. The original (obtained from FEM simulations) and the fitted series impedance values, magnitude and angle, for the 7th turn (the middle turn of the coil) are shown in Fig. 7 and Fig. 8, respectively. As can be seen, the frequency responses match very well, hence, the model is considered suitable to take the high-frequency characteristic of the coil into account.

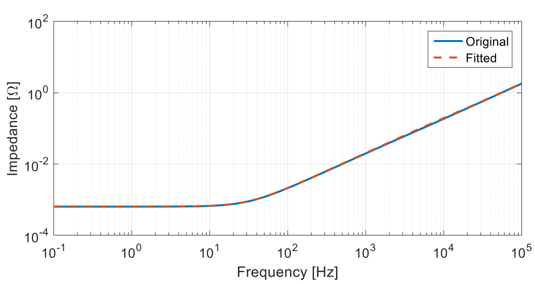

Fig. 7. Series impedance amplitude of the 7th turn for the end-windings.

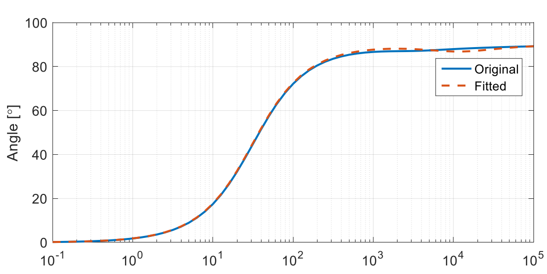

Fig. 8. Series impedance angle of the 7th turn for the end-windings.

B. Stator Core

The geometry simulated in the magnetic transient solver presented in Fig. 1 is related to the stator core, therefore, for this region, regarding the series impedance, that is, the inductances and resistance, they are already included. To take the proximity and eddy current effects into account, the 2D geometry considers each stranded conductor modelled individually. Moreover, the core model considers the non-linear BH curve (where B is de magnetic flux density and H is the magnetic field intensity), and also the frequency-dependent losses due to, for instance, the hysteresis and eddy current effects, which permits to consider the penetration reduction of the magnetic field into iron as the frequency increases. Moreover, all the inductive coupling between all the turns of the three phases is considered.

Therefore, for the stator core, only the stray capacitances need to be calculated. Due to the symmetry in this region, they are calculated using a 2D geometry. The model is comprised by a single coil in the slot region.

The parameters used in electrostatic solver simulation for slot region are the same of those used for end-windings region. The main difference is that the entire external surface of the coil is considered grounded in this region, because of the presence of the partially conductive coating [13]. Moreover, the stator core is also considered grounded as usual in real machines. Capacitance values obtained for the slot region are also presented in TABLE IV. According to the results, the mutual capacitances per unit length are similar for both regions. However, the turn-to-ground capacitances are much higher for the slot region, because the external surface of the coil is grounded in all extension of the stator core length.

C. Rotor Model

For the rotor, as presented in Fig. 3, the model of the bars is already included in the FEM geometry, nevertheless, it is missing the end rings and stray capacitances.

Firstly, in relation to the series impedance, the end rings are modelled as frequency-dependent as depicted in Fig. 9.

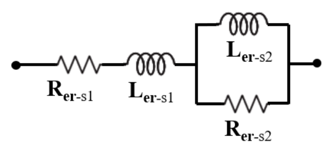

Fig. 9. Frequency-dependent model for end rings.

The parameters (R_{er-s1}, R_{er-s2}, L_{er-s1}, and L_{er-s2}) are calculated as done for the end-windings region, which means that the resistance and inductance as a function of the frequency are used to fit the series impedance. Therefore, the first step is to build the end-rings geometry. Due to the symmetry a 2D axisymmetric geometry can be used, as shown in Fig. 10.

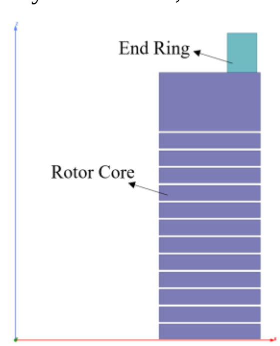

Fig. 10. Geometry used to calculate the end-ring series impedance.

Using an eddy-current simulation, the inductance and resistance of the end rings are obtained as shown in Fig. 11 and Fig. 12, respectively. From the extreme values of resistance and inductance of the curves presented in Fig. 11 and Fig. 12, respectively, the parameters of the model presented in Fig. 9 can be calculated using the same methodology detailed in the end-windings model.

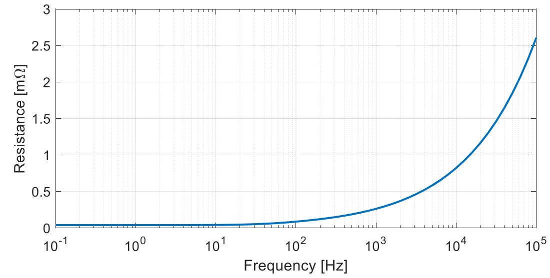

Fig. 11. End-ring' resistance as a function of frequency.

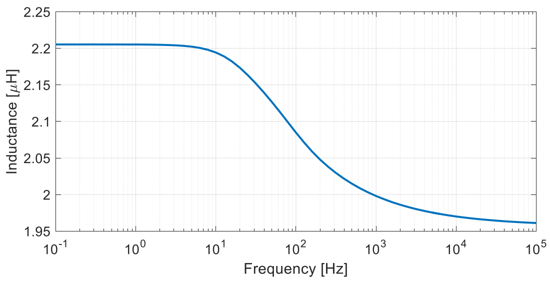

Fig. 12. End-ring' inductance as a function of frequency.

The comparison between the original series impedance (obtained from FEM simulations) and the fitted one, can be seen in Fig. 13 and Fig. 14 for the amplitude and angle, respectively. According to the figures, the results match well, and the model is suitable.

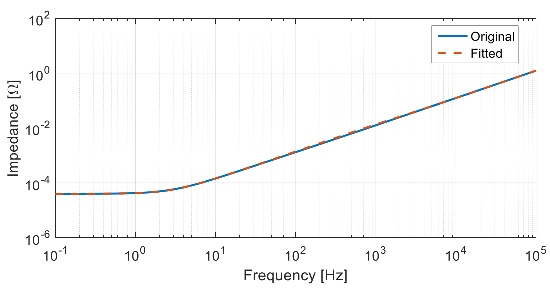

Fig. 13. Series impedance amplitude of the end ring.

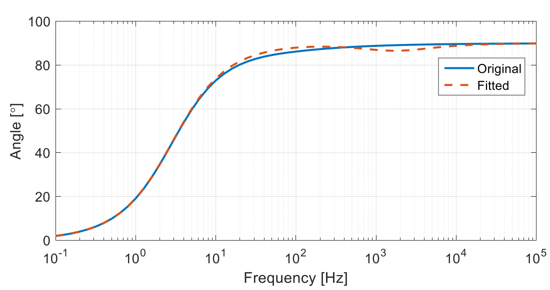

Fig. 14. Series impedance angle of the end ring.

Concerning the capacitances of the rotor to be included in the model, according to [16] the applicable values are related to the rotor-to-stator core (or rotor-to-ground) and to the rotor-to-stator coils. There are no capacitances between the bars of the rotor, since the rotor core is conductive and the rotor bars do not have insulation, they can be considered at the same potential. Therefore, the simulations in the electrostatic solver are carried out to calculate the applicable capacitances by using a 2D geometry

The complete geometry of the rotor and the stator core are considered to obtain the rotor-to-ground (rotor-to-stator core) capacitances. Moreover, two coils (one on the top and other on the bottom of the slot) of the stator winding are considered to calculate the capacitance from rotor-to-stator coils. For both coils the main and turn insulations are considered. The results can be seen in TABLE IV. According to the simulations, the rotor-to-stator coils capacitances can be disregarded, since they are much lower than the rotor-to-ground ones. Moreover, the capacitance from each bar-to-ground shown in TABLE IV, which is used in the model presented in Fig. 3, is considered as the total rotor-to-ground capacitances divided by the number of rotor bars.

TABLE IV
CAPACITANCE RESULTS.

Region	Capacitance	Value [pF]
Stator-Core	Turn-to-Ground – First and Last Turns	166.1
	Turn-to-Ground – Middle Turns	539.8
	Turn-to-Turn	1204.9
End-Windings	Turn-to-Ground – First and Last Turns	132.5
	Turn-to-Ground – Middle Turns	40.8
	Turn-to-Turn	1001.7
Rotor	Bar-to-Ground	48.4

III. MODEL VALIDATION

The validation of the model for the stator windings presented in the last section is done in this section. The capacitances-to-ground measured for one coil and the transient waveform obtained during the surge test of one individual coil are compared with those results simulated using the FEM model.

A. Capacitances of the Stator

The values of the capacitances-to-ground per coil are compared with those measured during the tan delta test [17]. In TABLE IV the results obtained for capacitances-to-ground calculated for each stator turn are shown for both regions, end-windings and stator-core. To obtain the total capacitance per coil is necessary to sum the values for all turns. The comparison of both results, simulated and measured, is depicted in TABLE V, which shows a good agreement between the values.

TABLE V
VALIDATION OF MACHINE WINDING CAPACITANCES.

Calculated [pF]	Measured [pF]	Error [%]
4333.7	4010.1	8.1

B. Stator Windings Transient Model

To validated the transient model, the high frequency waveform obtained by the FEM model is compared with the surge test [18] result measured for a single coil. The simulation and the measure have been performed with the coil inserted in the stator to consider the influence of the core. The procedure used during the surge test can be described by the scheme depicted in Fig. 15. The source of the surge tester charges the capacitance C_S from zero to the voltage test when the switch (S) closes and the energy is discharged in the coil. As main result a damped oscillatory waveform is created, whose frequency depends on the coil high-frequency parameters. To validate the FEM model the same procedure has been simulated, which means that the 13 turns inserted in the stator core have been considered. The comparison of the waveforms, measured and simulated, is shown in Fig. 16. As can be seen the transient responses match very well and the model is considered suitable for high frequency studies.

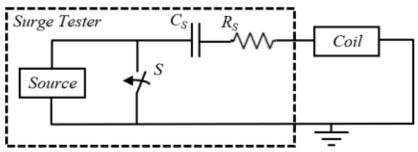

Fig. 15. Scheme for surge test procedure.

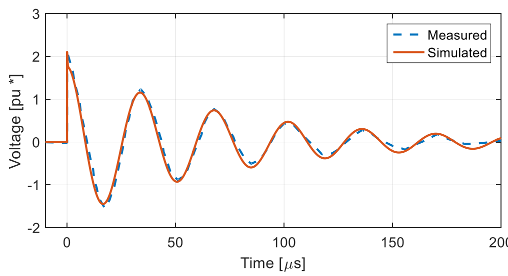

Fig. 16. Validation of the transient model (* per unity of the peak line-to-ground voltage).

IV. Transient Simulations

To verify the rotor influence, numerical simulations were performed using the model described in the previous section. The simulations consider one of the four existent group of coils. The surge is applied in the line-end coil from phase "a" and the line-end coils of phases "b" and "c" are grounded, as shown in Fig. 17.

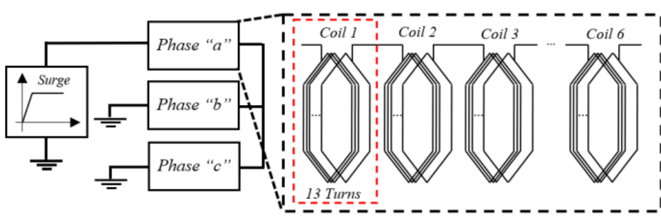

Fig. 17. Coils arrangement for simulations.

The simulations have been performed using a ramp function with amplitude (V_{AP}) equal to 100 V and a rise time equal to 0.2 μs. The objective is to compare the turn-to-turn and turn-to-ground voltages, considering (Case 1) and neglecting (Case 2) the rotor model, for all the turns of the tree phases, which means that the voltages for the 78 turns of each phase are analysed. All results are in the percentage of the applied voltage (% of V_{AP}). The voltage waveforms are presented only for phase "a" because it is where the highest overvoltages are found. However, the peak values are compared for the three phases. The turn-to-turn and turn-to-ground waveforms are presented in Fig. 18 and Fig. 19, respectively, and they are related to the last turns within each coil form phase "a".

The waveforms are a result of the interaction of many reflected waves occurring in the machines junctions, for instance, in the same coil (stator-core – end-windings – stator core) and in the star-point connection. Hence, to take all the junctions account a three-phase model is required.

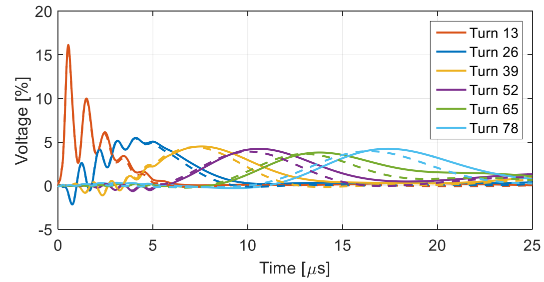

Fig. 18. Turn-to-turn voltage distribution for phase "a" (Case 1: solid lines and Case 2: dashed lines).

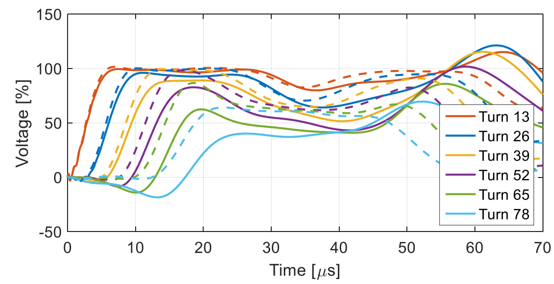

Fig. 19. Turn-to-ground voltage distribution for phase "a" (Case 1: solid lines and Case 2: dashed lines).

According to the results it can be seen that the voltages in each turn are shifted by the time that the surge takes to propagate between the turns. Moreover, the highest turn-to-turn overvoltage is found in the turn belonging to the first coil (Turn 13). In relation to the influence caused by the rotor, for both voltages, turn-to-turn and turn-to-ground, two points are observed: the shift between the turns are reduced, especially for the other than the 13th and; the peak values are also reduced. The main explanation is due to the additional parameters imposed by the rotor (resistance, inductance and capacitances) and also the additional coupling between stator and rotor, which affect the surge impedance of each coil.

The comparison of the peak values for the three phases are presented in Fig. 20 and Fig. 21 for turn-to-turn and turn-to-ground voltages, respectively.

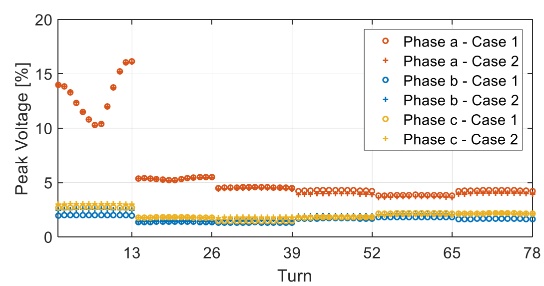

Fig. 20. Turn-to-turn voltage peak comparison.

As can be seen, in phase "a" for the first turns the values are almost the same, hence the rotor has low influence. For the other turns from phase "a" and all turns of phases "b" and "c", the differences are higher but still not very relevant for the turn insulation design, which is based on the highest value from the three phases. Nevertheless, regarding the turn-to-ground results, which are related to the main insulation design, the peak values are lower for all the turns from phase “a” when the rotor is considered. For phases “b” and “c”, in general, the voltages are higher when the rotor is considered.

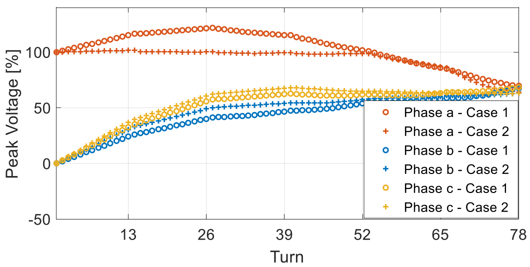

Fig. 21. Turn-to-ground voltage peak comparison.

Finally, in TABLE VI and in TABLE VII the maximum values found for each phase are compared for both cases, with and without the rotor. Regarding the results for phase “a”, which are those that define the thickness of the insulations, the variation of the turn-to-turn value is negligible. However, the he turn-to-ground overvoltage is reduced by 16.4% when the rotor is considered, which is an important margin when an optimized insulation is required.

TABLE VI
Maximum turn-to-turn voltages.

Phase	**Case 1 [%]**	**Case 2 [%]**	**Variation [% of Case 1]**
a	16.1	16.06	-0.5
b	2.0	2.6	26.2
c	2.7	3.1	12.6

TABLE VII
MAXIMUM TURN-TO-GROUND VOLTAGES.

Phase	**Case 1 [%]**	**Case 2 [%]**	**Variation [% of Case 1]**
a	121.7	101.7	-16.4
b	67.7	63.1	-6.9
c	68.2	68.1	-0.1

V. CONCLUSIONS

In this paper a three-phase model to study transient voltage distribution in stator windings of rotating machines taking the rotor into account has been proposed. The model presented consider all coils of one winding group and the rotor, which is normally not found in the literature, once the turn-based models found only consider part of the winding without the rotor. The frequency dependence of the stator core, end-windings and rotor, for instance, proximity and eddy effects, are take into account. The model of each individual coil of the stator has also been validated by experimental results.

Turn-to-ground and turn-to-turn voltages have been evaluated, once they are important to design the main and turn insulations. Simulations with and neglecting the rotor are carried out. Regarding the turn-to-turn overvoltages, the highest values are found in the first coil, which are much higher than those found for all remaining turns. In relation to the rotor dependence, it can be noted that for the first two coils of phase “a” the voltages are similar for both cases and for the remaining turns higher differences are found, but they do not affect the turn insulation design. For the turn-to-ground an important reduction (16.4%) of the maximum overvoltages has been found, which influences the main insulation design.

Therefore, a three-phase model considering the rotor is suggested to be used, especially in optimized insulation designs, in which the model shall be as exact as possible.

The three-phase model presented in this paper will be used in a future work to study the transient voltage distribution during the motor energization by considering the second pole closure, which generates the highest stresses in the insulation.

VI. REFERENCES

[1] L. Benmamas, P. Teste, E. Odic, G. Krebs and T. Hamiti, “Contribution to the analysis of PWM inverter parameters influence on the partial discharge inception voltage,” in IEEE TDEIS, vol. 26, no. 1, pp. 146-152, Feb. 2019.

[2] G. C. Stone and I. Culbert, “Partial discharge testing of random wound stators during short risetime voltage surges,” 2009 IEEE EIC Montreal, QC, 2009, pp. 188-191.

[3] Zhang et al., “Analysis of Inter-Turn Insulation of High Voltage Electrical Machine by Using Multi-Conductor Transmission Line Model,” in IEEE TMAG, vol. 49, no. 5, pp. 1905-1908, May 2013.

[4] H. De Gersem, O. Henze, T. Weiland and A. Binder, “Transmission-line modelling of wave propagation effects in machine windings,” 13th IPEMCC, Poznan, 2008, pp. 2385-2392.

[5] M. K. Hussain and P. Gomez, "Optimized dielectric design of stator windings from medium voltage induction machines fed by fast front pulses," in IEEE TDEIS, vol. 24, no. 2, pp. 837-846, April 2017.

[6] Krings, G. Paulsson, F. Sahlén and B. Holmgren, “Experimental investigation of the voltage distribution in form wound windings of large AC machines due to fast transients,” 2016 XXII ICEM, Lausanne, 2016, pp. 1700-1706.

[7] K. J. Cornick and T. R. Thompson, “Steep-fronted switching voltage transients and their distribution in motor windings. Part 2: Distribution of steep-fronted switching voltage transients in motor windings,” in IEE Proceedings B - EPA, vol. 129, no. 2, pp. 56-63, March 1982.

[8] M. T. Wright, S. J. Yang and K. McLeay, “General theory of fast-fronted interturn voltage distribution in electrical machine windings,” in IEE Proceedings B - EPA, vol. 130, no. 4, pp. 245-256, July 1983.

[9] W. W. L. Keerthipala and P. G. McLaren, "The effects of laminations on steep fronted surge propagation in large AC motor coils," in *IEEE TEC*, vol. 5, no. 1, pp. 84-90, March 1990.

[10] H. Oraee and P. G. McLaren, "Interturn voltage stress in electrical machine windings due to fast switching surges," *CEI&DP - Annual Report 1984*, Claymont, DE, USA, 1984, pp. 561-566.

[11] W. N. Fu, P. Zhou, D. Lin, S. Stanton and Z. J. Cendes, “Modelling of solid conductors in two-dimensional transient finite-element analysis and its application to electric machines” in IEEE TMAG, vol. 40, no. 2, pp. 426-434, March 2004.

[12] R. S. Ferreira and A. C. Ferreira, “Transient Voltage Distribution in Induction Motor Stator Windings Using Finite Elements Method,” IECON 2018 - 44th Annual Conference of the IEEE IES, Washington, DC, 2018, pp. 737-742.

[13] R. S. Ferreira and A. C. Ferreira, “End-Windings Modelling to Study Transient Voltage Distribution in Induction Motor Stator Windings Using Finite Elements Method,” IPST, 2019, Perpignan, France.

[14] A. F. Moreira, T. A. Lipo, G. Venkataramanan and S. Bernet, "High-frequency modeling for cable and induction motor overvoltage studies in long cable drives," in *IEEE TIAS*, vol. 38, no. 5, pp. 1297-1306, Sept.-Oct. 2002.

[15] L. Wang, C. Ngai-Man Ho, F. Canales and J. Jatskevich, "High-Frequency Modeling of the Long-Cable-Fed Induction Motor Drive System Using TLM Approach for Predicting Overvoltage Transients," in *IEEE TPE*, vol. 25, no. 10, pp. 2653-2664, Oct. 2010.

[16] A. Muetze and A. Binder, “Calculation of Motor Capacitances for Prediction of the Voltage Across the Bearings in Machines of Inverter-Based Drive Systems,” in IEEE TIAS, vol. 43, no. 3, pp. 665-672, May-june 2007.

[17] IEEE Std 286, “Recommended Practice for Measurement of Power Factor Tip-Up of Electric Machinery Stator Coil Insulation,” in IEEE Std 286-2000, vol., no., pp.1-29, 1 March 2000.

[18] IEEE Std 522, “Guide for Testing Turn-to-Turn Insulation on Form-Wound Stator Coils for Alternating-Current Rotating Electric Machines,” 2004.